JACS
JOURNAL OF THE AMERICAN CHEMICAL SOCIETY
Communication
pubs.acs.org/JACS

Surfactant-Directed Atomic to Mesoscale Alignment: Metal Nanocrystals Encased Individually in Single-Crystalline Porous Nanostructures

Pan Hu,[†,∥] Jia Zhuang,[†,∥] Lien-Yang Chou,[†] Hiang Kwee Lee,[‡] Xing Yi Ling,[‡] Yu-Chun Chuang,[§] and Chia-Kuang Tsung*[,†]

[†]Department of Chemistry, Merkert Chemistry Center, Boston College, Chestnut Hill, Massachusetts 02467, United States
[‡]Division of Chemistry and Biological Chemistry, School of Physical and Mathematical Sciences, Nanyang Technological University, Singapore 637371
[§]National Synchrotron Radiation Research Center, Hsinchu 30076, Taiwan

Supporting Information

ABSTRACT: Composite nanomaterials are attractive for a diverse range of applications in catalysis, plasmonics, sensing, imaging, and biology. In such composite nanomaterials, it is desired, yet still challenging to create a controlled alignment between components with lattices in disparate scales. To address this challenge, we report a new concept of colloidal synthesis, in which self-assembled molecular layers control the alignment between materials during the synthesis. To illustrate this concept, self-assembled cetyltrimethylammonium bromide (CTAB) molecules are used to control interfaces in a core−shell nanocomposite with a well-defined metal nanocrystal core and a metal−organic-framework (MOF) shell, which differ in structural dimensions by orders of magnitude. We show that single metal nanocrystals are captured individually in single-crystalline MOFs, and an alignment between the {100} planes of the metal and {110} planes of the MOFs is observed. By utilizing the same concept, a layer of mesostructured silica is formed over MOF crystals. These multilayered core−shell structures demonstrate a controlled alignment across a wide range of materials, from the metal nanocrystals, extending to nanoporous MOFs and mesostructured silica.

A controlled alignment at the interface between materials across a wide range of size scales is critical to composite materials. It is especially essential to composite nanomaterials as their interfaces exist in the mesoscale, where classical physics, quantum mechanics, and nanoscience meet.[1,2] However, interfacial control in nanomaterials is challenging because of the requirement of atomic-level alignment, which is hindered by large interfacial energies between materials with crystal lattices in different scales, such as metal lattices and the microporous structure of zeolites.[3] This is true for even the simplest construction, a core−shell nanostructure.[4−6]

Core−shell nanocomposites with catalytic cores and porous shells are particularly attractive because porous shells[7−9] can prevent aggregation[10] as well as provide enhanced selectivity and reactivity.[11,12] Although interfacial control between the core and shell of such structures has not yet been studied, it is logical to believe that a controlled alignment at the interface can provide a more precise control of the diffusion, sorption, and orientation of molecules during catalytic reactions.[13,14] Thus, in this work, we use a core−shell nanocomposite structure with a core of well-defined metal nanocrystal and a shell of single-crystalline nanoporous metal−organic frameworks (MOFs)[15,16] as an archetype to study the alignment between the core and shell (Scheme 1). This proof-of-concept system is not only representative because of the significant lattice differences between metal and nanoporous materials but also because well-aligned interfaces could enable new functions to core−shell nanomaterials.

Scheme 1. Formation of Nanocrystals Encased Individually and Aligned in Single-Crystalline Porous Materials[a]

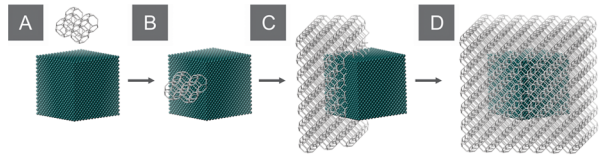

[a](A) Introduction of well-defined nanocrystals after the nucleation of ZIF-8. (B) Single-crystalline ZIF-8 nucleus attachment to the metal surface with selective orientation. (C) ZIF-8 crystal growth on the nucleus. (D) Single nanocrystal captured in single crystalline ZIF-8 with lattice alignment.

Here, we utilize ionic surfactant molecules, cetyltrimethylammonium bromide (CTAB), to bridge the metal and zeolitic-imidazolate-framework-8 (ZIF-8) surfaces and to facilitate the controlled alignment. The nanocrystal@MOF core−shell nanocomposites synthesized here are composed of single shape-controlled metal nanocrystals individually encased in ZIF-8 nanocrystals (Figure 1). Previous studies have shown that the addition of polymer molecules could promote the overgrowth;[18,19] however, due to the polymer nature of PVP molecules, controlled alignment was not observed. Meanwhile, using highly ordered self-assembled alkanethiol molecular layers

Received: May 15, 2014
Published: July 9, 2014

   dx.doi.org/10.1021/ja5048522 | J. Am. Chem. Soc. 2014, 136, 10561−10564

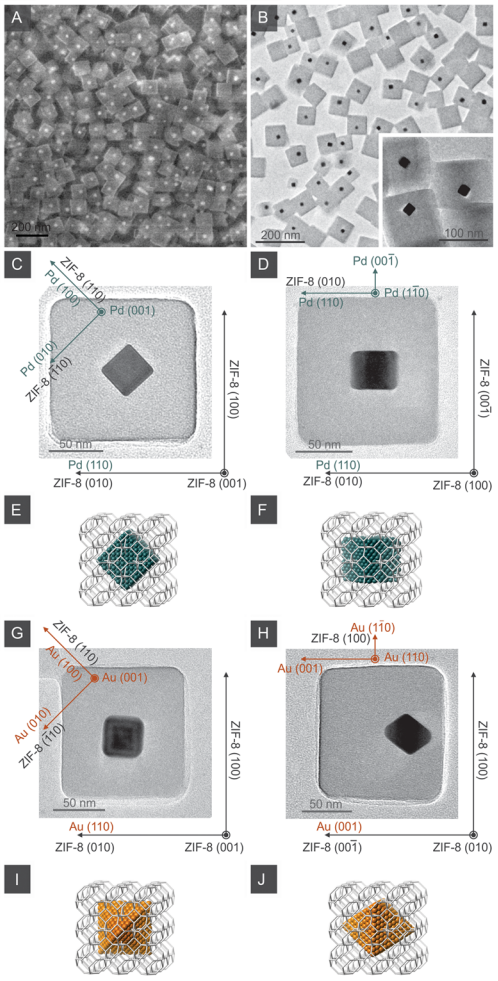

Figure 1. TEM and SEM images of metal nanocrystal@ZIF-8 and corresponding 3D projection models. (A) SEM image of core−shell Pd@ZIF-8 nanocomposites. (B) TEM image of core−shell Pd@ZIF-8 nanocomposites. (C,D) TEM images of Pd cube@ZIF-8 in [001] and [100] view directions. (E,F) 3D modeling projections of C and D, respectively. (G,H) TEM images of Au octahedron@ZIF-8 in [001] and [010] view directions. (I,J) 3D projection models of G and H, respectively.

to align the overgrowth on metal thin films has been extensively studied in the self-assembled monolayer (SAM) system.[20] We introduce this concept to our colloidal system, but instead choose CTAB molecules as they self-assemble to form layered structures on the surface of metal nanocrystals in aqueous solutions.[21] This CTAB molecular layer can bridge the interaction between metals and ZIF-8 by the hydrophobic tail, as well as stabilize specific facets of the metals and MOFs,[22,23,24] so an alignment between the crystal structures of the cores and shells is expected.

Capturing nanoparticles in MOFs has drawn much attention over recent years.[25−30,31,32] The integration of the nanoparticle properties with the advantages of MOFs provides a new tool to create multifunctional materials for gas adsorption/storage,[33] sensing,[34] heterogeneous catalysis,[29] drug delivery,[35] and pollution sequestration.[36] Several methods have been developed. Fischer et al. adopted the gas-phase infiltration method[37] and Xu et al. developed the liquid-phase impregnation approach.[33,38−40] Sada, Huo, Tang, and Furukawa introduced preformed nanoparticles into MOF synthetic precursors[19,41−45] and our group developed a method to generate yolk−shell nanocomposites.[11] Despite the success of these approaches, either multiple nanoparticles are captured in a large MOF crystal with random orientations[19,44] or a single nanoparticle is encased in a shell composed by granular MOF crystals.[34,42] The structure of nanoparticles individually encased in single-crystalline MOF crystals in a one-to-one structure has not been achieved, to say nothing of a controlled alignment between the lattices of nanoparticles and MOFs.

Aqueous phase syntheses using CTAB for both metal and ZIF-8 nanocrystals were first explored and optimized separately, in order to have the ordered self-assembled layer of CTAB.[24,46,47] The scanning electron microscopy (SEM) and transmission electron microscopy (TEM) images show that the uniform cubic Pd, Au, and ZIF-8 nanocrystals were synthesized (Figure S1). The Pd and Au cubes are ∼30 and ∼50 nm, respectively. The crystal sizes of ZIF-8 can be tuned from ∼60 to ∼150 nm by varying the CTAB amount. The cubic structure enclosed by six {100} facets was chosen because this simple geometric morphology can benefit the exploration of the alignment. The Pd and Au are selected because of their respective catalytic and plasmonic properties. To synthesize nanocrystal@ZIF-8 core−shell nanocomposites, metal nanocrystals are synthesized first and then delivered to the ZIF-8 synthesis solution ∼10 s after the ZIF-8 precursors are mixed (Figure S2). The SEM and TEM images show that metal cubes are individually incorporated into the cubic single crystalline ZIF-8 crystals (Figures 1A,B). Nearly every MOF cube contains only one metal nanocrystal, and the nanocomposites are of narrow size distribution. Few, if any, free metal nanocrystals were found outside the MOFs. A small number of empty ZIF-8 cubes were found but could be removed by centrifugation. The morphology of the metal cubes was maintained, and no sintering or etching was observed. By varying the CTAB amount, the ZIF-8 shell thicknesses were tuned from ∼35 to 60 nm (Figure S3). This thickness control could be used for molecular diffusion studies in the future. The crystal structures and chemical compositions of the core−shell nanocomposites were confirmed by powder X-ray diffraction (PXRD) (Figure S4) and inductively coupled plasma optical emission spectroscopy (Table S1). Size selective hydrogenations of alkenes were carried out to confirm that the metal nanocrystals were encased in ZIF-8.[11] The Pd@ZIF-8 nanocomposites were compared with a control sample containing the same amount of Pd deposited on the external surface of ZIF-8 crystals (Table S2). After intensive washing for the removal of CTAB, both samples show activities in ethylene hydrogenation because of the small size of ethylene molecules. No activity was observed for cyclooctene hydrogenation over the Pd@ZIF-8 sample, while appreciable activity was observed over the control sample because the size of cyclooctene molecules is much larger than the aperture size of ZIF-8. The selective hydrogenation results reveal the metal nanocrystals are encased in ZIF-8 and that no fracture or fragmentation exists in the single crystalline ZIF-8 shell.

The alignment between metal nanocrystals and ZIF-8 is explored by the magnified TEM images (Figures 1 and S5). Because both metal and ZIF-8 cubes are enclosed by six {100} surfaces, it is relatively easy to reveal the lattice alignment according to the relative orientations between the two. Most of the nanocomposites show the same alignment. Figure 1C,D shows two view directions of this alignment, two sets of {100} planes of the metal align with two sets of {110} planes of ZIF-8. Models of the projections in the [100] and [010] view directions of ZIF-8 are in accordance with the TEM images. To further

dx.doi.org/10.1021/ja5048522 | J. Am. Chem. Soc. 2014, 136, 10561−10564

investigate the alignment, we extended the method to cores with octahedral morphology. Au octahedra (~50 nm) are used, and to our surprise, the {100} metal planes still align with the ZIF-8 {110} planes although the octahedra are mainly enclosed by eight {111} surfaces. Two view directions are shown in Figures 1G and 1H. In the ZIF-8 [100] and [010] view directions, the respective rhombic and square-shaped cross sections with radial patterns along the diagonal were observed. About 20% of the nanocomposites are of alignment of the metal {100} planes with ZIF-8 {100} planes (Figures S5 and S6). We did not observe any alternate alignment orientations.

To the best of our knowledge, our nanocrystal@ZIF-8 nanocomposite is the first example that has this specific lattice alignment between the metal core and porous shell. We believe the self-assembled CTAB layer and the time of metal NP introducing are critical. The proposed mechanism is illustrated in Scheme 1. Small ZIF-8 nuclei enclosed by low surface energy {110} facets form in the solution first. Then a single ZIF-8 nucleus attaches via the bridging CTAB layer to a single metal NP and generates a ZIF-8 {110} to metal {100} interface. The rest of the ZIF-8 shell grows exclusively on this orientated crystal nucleus to capture the metal nanocrystal, instead of through a layer-by-layer conformal overgrowth mechanism. This one-core-to-one-nucleus attachment leads the one-in-one single-crystalline structure. Due to the small energy difference between {110} and {100} of ZIF-8, a small portion of {100} to {100} alignment is also formed. The key step of this mechanism, ZIF-8 nucleus selective attachment to the metal {100} facet, is reasonable in the metal cube case because of the dominant {100} facets of the metal cubes; however, we ask the question, why does the {100} selective attachment still occur in the case of a metal octahedron? The octahedral geometry allows for a few, small {100}-terminated surfaces, these of which are exclusively located at the vertices and arise from truncation due to the increase in under-coordinated (higher surface energy) atoms at the apex.[48] The {100} metal facets may still serve as the attachment site for the ZIF-8 nucleus, despite their limited abundance. The highly selective attachment can be explained by the result of extensive studies in SAM system.[49] Huo et al. has shown that the ZIF-8 nucleus on the SAM is sensitive to the metal surface because the orientation of nuclei is determined by the distance between the self-assembled molecules and the distance of the molecules is determined by the surface metal lattices. In our case, CTAB self-assembled layers on the metal {100} facets might have a more ideal structure compared to other facets for the nucleus attachment.

To support this proposed mechanism, a series of control experiments were carried out. First, octahedron@ZIF-8 at different reaction stages were examined by TEM (Figure 2A–C). In the early stage, a small ZIF-8 nanocrystal is attached to the vertex of a Au octahedron, and a certain degree of alignment is already present. As the growth continued, the alignment was preserved and eventually led to the formation of core–shell nanocomposites with the interface alignment. Surface-enhanced Raman scattering (SERS) was carried out during the synthesis of Au octahedron@ZIF-8 to reveal the existence of CTAB layer at different stages. At the different stages, we have observed similar intensities of the most intense SERS signal, CH_2 twisting mode of CTAB at 1266 cm^{-1} (Figure 2E,F). As the SERS intensity is dependent on the amount of probe molecules present on the surface of Au, the amount of CTAB near the surfaces of the Au octahedra remained unchanged throughout the reaction. Second, metal nanocrystals capped by PVP instead of CTAB in methanol

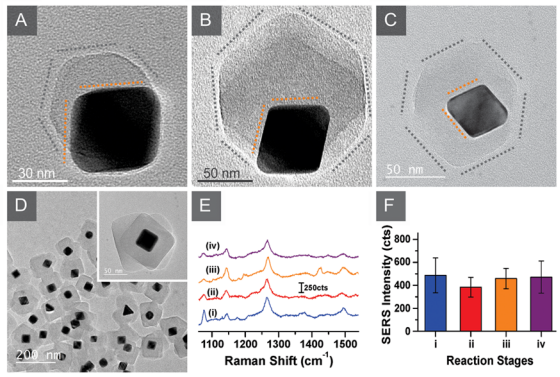

Figure 2. (A–C) TEM images of Au octahedron@ZIF-8 at different reaction stages, A: 1 min, B, C: 2 min. (D) Polycrystalline ZIF-8 shell when mixing nanocrystals and ZIF-8 precursors simultaneously. (E,F) SERS signals of CTAB during different reaction stages, (i) Au octahedra before reaction, (ii) partial encapsulation of Au octahedra with ZIF-8 (40 min), (iii) Au@ZIF-8 (120 min), and (iv) complete acid-induced disintegration.

solution were used. Multiple nanocrystals were encapsulated in one large ZIF-8 crystal, and no specific alignment was observed.[11,19] Third, when the metal nanocrystals and precursors of ZIF-8 were mixed simultaneously, the encapsulation was still observed but polycrystalline ZIF-8 shells were obtained (Figure 2D). This is explained by that when the metal nanocrystals are introduced before the formation of crystalline nuclei, the amorphous nuclei randomly attached on the metal surfaces and eventually lead to the formation of polycrystalline ZIF-8 shells.

To demonstrate the generality of this concept, CTAB was used to further direct the overgrowth of the MCM-41 type mesostructured silica on ZIF-8 (Figure S7).[50,51] We believe the self-assembled CTAB molecules serve as a structure directing agent of the mesostructure and also bridge the mesostructured silica and nanoporous ZIF-8. By adding tetraethyl orthosilicate (TEOS) into the colloidal Pd@ZIF-8 nanocomposite solution with the presence of CTAB, a uniform layer of silica mesostructure overgrew on the ZIF-8 (Figure 3). Small-angle

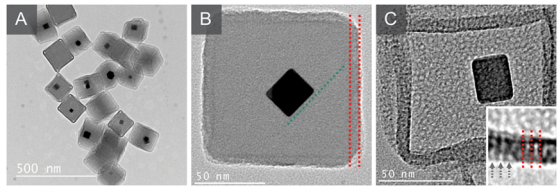

Figure 3. TEM images of (A,B) Pd@ZIF-8@mSiO_2 with alignment from atomic to mesoscopic scales and (C) composite with cylindrical mesostructured channels.

X-ray scattering patterns confirm the crystal structure of the metal, nanoporous structure of ZIF-8, and mesostructure of silica (Figure S8). In the absence of CTAB molecules, the formation of either solid or mesostructured silica layer was not observed (Figure S9). After the removal of ZIF-8 by acid treatment, the cylindrical-oriented mesostructure was evident, which indicates the CTAB layer even provides a certain degree of alignment during the cooperative self-assembly of the mesostructure.[52]

In conclusion, with the assistance of self-assembling CTAB molecules, we have developed a new strategy to individually

dx.doi.org/10.1021/ja5048522 | J. Am. Chem. Soc. 2014, 136, 10561–10564

encase single metal nanocrystals into single-crystalline cubic ZIF-8 nanocrystals with a specific lattice alignment. A layer of mesostructured silica was deposed on the metal@ZIF-8 nanocomposite surface with alignment by the same strategy. To the best of our knowledge, this is the first example of the use of self-assembled molecules in colloidal syntheses to align crystalline materials from atomic to mesoscale. The alignment is essential for follow-up studies on the diffusion and orientation of molecules in such structures which will be investigated via spectroscopic analysis and catalysis experiments.

■ ASSOCIATED CONTENT

Supporting Information

Detailed experimental procedures; TEM images of nanocrystals; PXRD patterns of nanocomposites; elemental analysis; heterogeneous catalysis. This material is available free of charge via the Internet at http://pubs.acs.org.

■ AUTHOR INFORMATION

Corresponding Author

frank.tsung@bc.edu

Author Contributions

‖These authors contributed equally.

Notes

The authors declare no competing financial interest.

■ ACKNOWLEDGMENTS

This work is supported by Boston College. Thanks to Dr. C.-H. Kuo at Institute of Chemistry, Academia Sinica (Taiwan) and B. Sneed at Boston College for valuable discussion. Thanks to Prof. D. Qu and Dr. D. Zheng at UMass Boston for ICP-OES measurement. Thanks to Prof. S. Wilson at Boston College for the use of their diffractometer. Thanks also to G. McMahon for assistance with TEM and SEM.

■ REFERENCES

(1) Hemminger, J. *U.S. DOE Basic Energy Sciences Advisory Committee Report*; DOE: Washington, DC, 2012.
(2) Bowden, N. B.; Weck, M.; Choi, I. S.; Whitesides, G. M. *Acc. Chem. Res.* **2001**, *34*, 231.
(3) Bein, T. *Chem. Mater.* **1996**, *8*, 1636.
(4) Ghosh Chaudhuri, R.; Paria, S. *Chem. Rev.* **2011**, *112*, 2373.
(5) Zhang, Q.; Lee, I.; Joo, J. B.; Zaera, F.; Yin, Y. *Acc. Chem. Res.* **2012**, *46*, 1816.
(6) Guerrero-Martínez, A.; Pérez-Juste, J.; Liz-Marzán, L. M. *Adv. Mater.* **2010**, *22*, 1182.
(7) Sun, X.; Li, Y. *Angew. Chem., Int. Ed.* **2004**, *43*, 597.
(8) Teng, X.; Black, D.; Watkins, N. J.; Gao, Y.; Yang, H. *Nano Lett.* **2003**, *3*, 261.
(9) Wang, H.; Chen, L.; Feng, Y.; Chen, H. *Acc. Chem. Res.* **2013**, *46*, 1636.
(10) Joo, S. H.; Park, J. Y.; Tsung, C.-K.; Yamada, Y.; Yang, P.; Somorjai, G. A. *Nat. Mater.* **2009**, *8*, 126.
(11) Kuo, C.-H.; Tang, Y.; Chou, L.-Y.; Sneed, B. T.; Brodsky, C. N.; Zhao, Z.; Tsung, C.-K. *J. Am. Chem. Soc.* **2012**, *134*, 14345.
(12) De Rogatis, L.; Cargnello, M.; Gombac, V.; Lorenzut, B.; Montini, T.; Fornasiero, P. *ChemSusChem* **2010**, *3*, 24.
(13) Stallmach, F.; Gröger, S.; Künzel, V.; Kärger, J.; Yaghi, O. M.; Hesse, M.; Müller, U. *Angew. Chem., Int. Ed.* **2006**, *45*, 2123.
(14) Amirjalayer, S.; Tafipolsky, M.; Schmid, R. *Angew. Chem., Int. Ed.* **2007**, *46*, 463.
(15) Furukawa, H.; Cordova, K. E.; O'Keeffe, M.; Yaghi, O. M. *Science* **2013**, 341.
(16) Yaghi, O. M.; O'Keeffe, M.; Ockwig, N. W.; Chae, H. K.; Eddaoudi, M.; Kim, J. *Nature* **2003**, *423*, 705.
(17) James, S. L. *Chem. Soc. Rev.* **2003**, *32*, 276.
(18) Sun, H.; He, J.; Wang, J.; Zhang, S.-Y.; Liu, C.; Sritharan, T.; Mhaisalkar, S.; Han, M.-Y.; Wang, D.; Chen, H. *J. Am. Chem. Soc.* **2013**, *135*, 9099.
(19) Lu, G.; Li, S.; Guo, Z.; Farha, O. K.; Hauser, B. G.; Qi, X.; Wang, Y.; Wang, X.; Han, S.; Liu, X.; DuChene, J. S.; Zhang, H.; Zhang, Q.; Chen, X.; Ma, J.; Loo, S. C. J.; Wei, W. D.; Yang, Y.; Hupp, J. T.; Huo, F. *Nat. Chem.* **2012**, *4*, 310.
(20) Aizenberg, J. *Adv. Mater.* **2004**, *16*, 1295.
(21) Johnson, C. J.; Dujardin, E.; Davis, S. A.; Murphy, C. J.; Mann, S. *J. Mater. Chem.* **2002**, *12*, 1765.
(22) Lohse, S. E.; Burrows, N. D.; Scarabelli, L.; Liz-Marzán, L. M.; Murphy, C. J. *Chem. Mater.* **2013**, *26*, 34.
(23) Ortiz, N.; Skrabalak, S. E. *Langmuir* **2014**, ASAP.
(24) Pan, Y.; Heryadi, D.; Zhou, F.; Zhao, L.; Lestari, G.; Su, H.; Lai, Z. *CrystEngComm* **2011**, *13*, 6937.
(25) Moon, H. R.; Lim, D.-W.; Suh, M. P. *Chem. Soc. Rev.* **2013**, *42*, 1807.
(26) Liu, Y.; Tang, Z. *Adv. Mater.* **2013**, *25*, 5819.
(27) Foo, M. L.; Matsuda, R.; Kitagawa, S. *Chem. Mater.* **2013**, *26*, 310.
(28) Doherty, C. M.; Buso, D.; Hill, A. J.; Furukawa, S.; Kitagawa, S.; Falcaro, P. *Acc. Chem. Res.* **2013**, *47*, 396.
(29) Dhakshinamoorthy, A.; Garcia, H. *Chem. Soc. Rev.* **2012**, *41*, 5262.
(30) Jiang, H.-L.; Xu, Q. *Chem. Commun.* **2011**, *47*, 3351.
(31) Corma, A.; García, H.; Llabrés i Xamena, F. X. *Chem. Rev.* **2010**, *110*, 4606.
(32) Zhu, Q.-L.; Xu, Q. *Chem. Soc. Rev.* **2014**, Advance Article.
(33) Gu, X.; Lu, Z.-H.; Jiang, H.-L.; Akita, T.; Xu, Q. *J. Am. Chem. Soc.* **2011**, *133*, 11822.
(34) He, L.; Liu, Y.; Liu, J.; Xiong, Y.; Zheng, J.; Liu, Y.; Tang, Z. *Angew. Chem., Int. Ed.* **2013**, *52*, 3741.
(35) Zhuang, J.; Kuo, C.-H.; Chou, L.-Y.; Liu, D.-Y.; Weerapana, E.; Tsung, C.-K. *ACS Nano* **2014**, *8*, 2812.
(36) Ricco, R.; Malfatti, L.; Takahashi, M.; Hill, A. J.; Falcaro, P. *J. Mater. Chem. A* **2013**, *1*, 13033.
(37) Esken, D.; Zhang, X.; Lebedev, O. I.; Schroder, F.; Fischer, R. A. *J. Mater. Chem.* **2009**, *19*, 1314.
(38) Jiang, H.-L.; Akita, T.; Ishida, T.; Haruta, M.; Xu, Q. *J. Am. Chem. Soc.* **2011**, *133*, 1304.
(39) Aijaz, A.; Karkamkar, A.; Choi, Y. J.; Tsumori, N.; Rönnebro, E.; Autrey, T.; Shioyama, H.; Xu, Q. *J. Am. Chem. Soc.* **2012**, *134*, 13926.
(40) Zhu, Q.-L.; Li, J.; Xu, Q. *J. Am. Chem. Soc.* **2013**, *135*, 10210.
(41) Liu, Y.; Zhang, W.; Li, S.; Cui, C.; Wu, J.; Chen, H.; Huo, F. *Chem. Mater.* **2013**, *26*, 1119.
(42) Zhao, M.; Deng, K.; He, L.; Liu, Y.; Li, G.; Zhao, H.; Tang, Z. *J. Am. Chem. Soc.* **2014**, *136*, 1738.
(43) Khaletskaya, K.; Reboul, J.; Meilikhov, M.; Nakahama, M.; Diring, S.; Tsujimoto, M.; Isoda, S.; Kim, F.; Kamei, K.-i.; Fischer, R. A.; Kitagawa, S.; Furukawa, S. *J. Am. Chem. Soc.* **2013**, *135*, 10998.
(44) Sugikawa, K.; Nagata, S.; Furukawa, Y.; Kokado, K.; Sada, K. *Chem. Mater.* **2013**, *25*, 2565.
(45) Buso, D.; Nairn, K. M.; Gimona, M.; Hill, A. J.; Falcaro, P. *Chem. Mater.* **2011**, *23*, 929.
(46) Sneed, B. T.; Kuo, C.-H.; Brodsky, C. N.; Tsung, C.-K. *J. Am. Chem. Soc.* **2012**, *134*, 18417.
(47) Dovgolevsky, E.; Haick, H. *Small* **2008**, *4*, 2059.
(48) Seo, D.; Park, J. C.; Song, H. *J. Am. Chem. Soc.* **2006**, *128*, 14863.
(49) Li, S.; Shi, W.; Lu, G.; Li, S.; Loo, S. C. J.; Huo, F. *Adv. Mater.* **2012**, *24*, 5954.
(50) Beck, J. S.; Vartuli, J. C.; Roth, W. J.; Leonowicz, M. E.; Kresge, C. T.; Schmitt, K. D.; Chu, C. T. W.; Olson, D. H.; Sheppard, E. W.; McCullen, S. B.; Higgins, J. B.; Schlenker, J. L. *J. Am. Chem. Soc.* **1992**, *114*, 10834.
(51) Li, Z.; Zeng, H. C. *J. Am. Chem. Soc.* **2014**, *136*, 5631.
(52) Huo, Q. S.; Margolese, D. I.; Ciesla, U.; Feng, P. Y.; Gier, T. E.; Sieger, P.; Leon, R.; Petroff, P. M.; Schuth, F.; Stucky, G. D. *Nature* **1994**, *368*, 317.